Proceedings of CONF-MLA 2026 Symposium: Intelligent Systems and Automation: AI Models, IoT, and Robotic Algorithms
DOI: 10.54254/2755-2721/2026.LD39410

GWO-PD Attitude Control for the HErO Satellite in LED-Based Optical Communication Missions

ITO Naomi

Hiroo Gakuen Junior & Senior High School, Tokyo, Japan
itoapply@163.com

Abstract. Attitude control of spacecraft is an important aspect of satellite operation in orbit. It influences the stability of platform and payload. In this paper, attitude-pointing control of Hiroo Engineering for Orbit (HErO) satellite for Hiroo Gakuen satellite mission is studied. The LED optical communication payload is used to send the temperature data of circuit board to the ground station. The aim is to maintain the attitude pointing continuously throughout the orbit when it is visible to the ground experiment team through telescope. PD controller is used for attitude control of small satellites due to its simplicity in design and implementation. The controller gains have a great role in the response of the system. Hence, PD-parameter optimization technique using GWO is proposed. The attitude control system performance indices are studied. GWO is used to optimize the gains of proportional and derivative. The attitude dynamics model of HErO satellite is formulated. The proposed technique is simulated using MATLAB and Satellite Tool Kit (STK). The HErO satellite is able to point its LED surface steadily to the ground area in the simulation. The findings of the proposed technique show that it can improve the response and stability of the attitude control system. The paper can be used as a reference for the attitude control system of HErO satellite.

Keywords: Attitude Control, PD Controller, Grey Wolf Optimization, Attitude Pointing, Small Satellite

1. Introduction

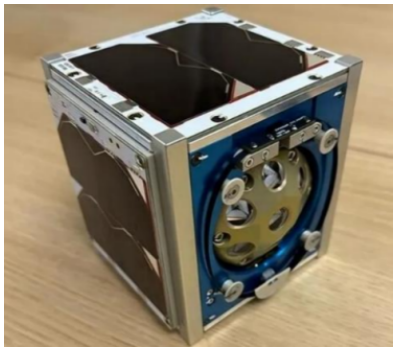


Figure 1. The HErO satellite designed by the student team at Hiroo Gakuen

© 2026 The Authors. This is an open access article distributed under the terms of the Creative Commons Attribution License 4.0 (https://creativecommons.org/licenses/by/4.0/).

DOI: 10.54254/2755-2721/2026.LD39410

HErO satellite is a CubeSat designed and implemented by a student of Hiroo Gakuen, Japan (see Figure 1). The mission shows optical communication using LED to send the temperature data of circuit board from outside of the satellite to ground station.

In order to observe the HErO satellite through telescope and receive the LED optical signal, the surface mounted with LED should be steadily pointed to the ground experiment team during the time when the satellite passes over the observation location. Without attitude control of the satellite after deployment in orbit, the satellite might tumble or drift in attitude. This is due to deployment disturbances, environmental torques and other perturbations. As a result, the satellite might not be able to point its LED-mounted surface to the required orientation to Earth. Hence, it is necessary to have an appropriate attitude controller according to the mission for the HErO satellite to operate properly. A PD controller is used as the structure of attitude control system of HErO satellite in this paper. The gains of the controller are optimised using Grey Wolf Optimisation (GWO) to improve the stability and response of the attitude control system. This is the outline of the rest of the paper. In section 2, the model of satellite attitude dynamics is formulated. Grey Wolf Optimization is discussed in section 3. In section 4, the PD gain optimisation using GWO is discussed. The proposed method is validated through the integrated MATLAB and Satellite Tool Kit (STK) simulations in section 5.

2. Satellite attitude dynamics modeling

During an internship at Mitsubishi Heavy Industries, the author also gained experience in ground-vehicle dynamics modeling and simulation. The motion of a conventional ground vehicle is generally constrained by the road surface. Therefore, a planar vehicle dynamics model is commonly used to describe changes in position velocity, and heading angle within the horizontal plane [1], as illustrated in Figure 2.

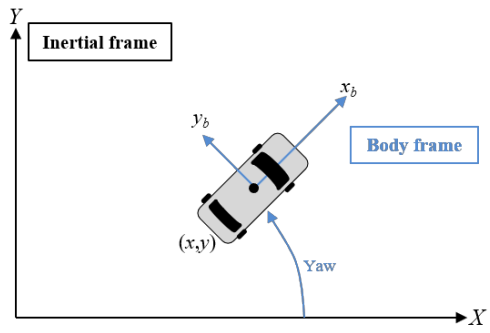


Figure 2. Two-dimensional planar pose representation of a ground vehicle

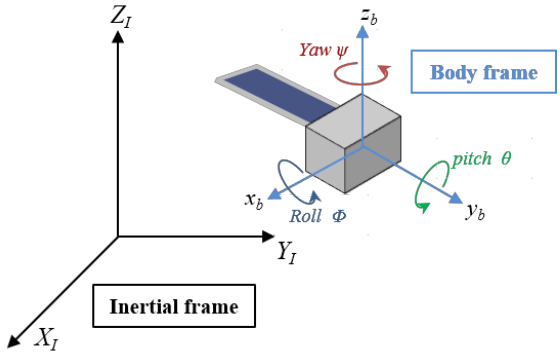


Figure 3. Three-dimensional attitude representation of a spacecraft

Further investigation shows that spacecraft attitude motion differs fundamentally from ground-vehicle motion because it involves three-dimensional rotation. A satellite operates in space without the constraints imposed by a ground surface. Its attitude describes the spatial orientation of the spacecraft body as it travels along its orbit. A body-fixed Cartesian coordinate system is defined with its origin located on the spacecraft. In this coordinate system, rotation about the X-axis represents roll, rotation about the Y-axis represents pitch, and rotation about the Z-axis represents yaw. Therefore, the spacecraft attitude must simultaneously describe rotational motion about all

DOI: 10.54254/2755-2721/2026.LD39410

three body axes, namely roll, pitch, and yaw, as illustrated in Figure 3. This section focuses on the modeling of spacecraft attitude dynamics.

2.1. Definition of coordinate systems

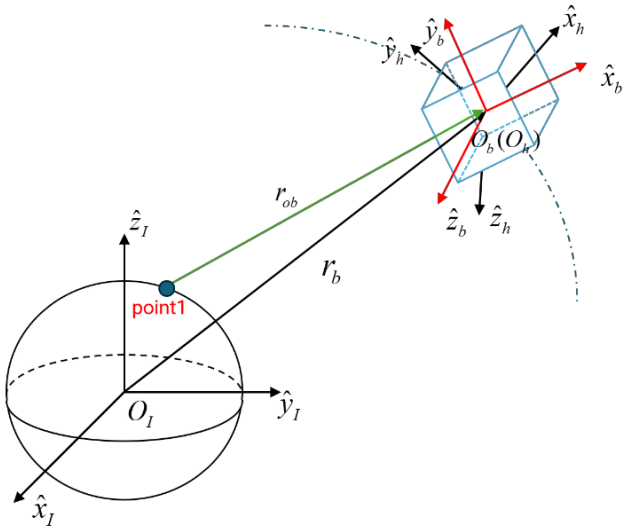


Figure 4. Reference coordinate frames for spacecraft motion

The coordinate systems adopted in this study are illustrated in Figure 4.

2.1.1. Earth-centered inertial frame OI

The Earth's center is where the origin is situated. The Zi-axis is parallel to the tropical plane and points in the direction of the North Pole, while the Xi-axis points in the direction of the vernal equinox. The right-hand rule is used to identify the Yi-axis [2].

2.1.2. Orbital frame Oh

The center of mass of the spaceship is where the origin is situated. The Xh-axis points from the Earth's center in the direction of the spacecraft and is aligned with the position vector rb. Perpendicular to the Xh-axis, the Yh-axis is located in the orbital plane. The spacecraft's motion is in line with its positive direction. Along with the Xh and Yh axes, the Zh axis forms a right-handed coordinate system and is normal to the orbital plane.

2.1.3. Spacecraft body-fixed frame Ob: ObXb YbZb

The center of mass of the spaceship is where the origin is situated. The Xb, Yb, and Zb axs line up with the spacecraft's primary axs of inertia. The LED-mounted surface of the satellite considered in this study has an outward normal aligned with the positive Zb-axis.

2.2. Attitude dynamics modeling

The spacecraft attitude dynamics are described by the following equations:

DOI: 10.54254/2755-2721/2026.LD39410

$$\frac{d_I H}{dt} = \frac{d_B H}{dt} + w \times H = T \tag{1}$$

where dI and dB denote the time derivatives evaluated in the inertial and body- fixed frames, respectively. Therefore,

$$H = Tw \qquad w = J_1H \tag{2}$$

where T is the control torque applied to the spacecraft, J is the spacecraft inertia matrix, where w is the body-fixed frame's angular velocity vector with respect to the inertial frame.

2.3. Attitude kinematics modeling

In the study of spacecraft attitude kinematics, Euler angles provide an intuitive representation of spacecraft attitude, as illustrated in Fig. 3. However, the Euler-angle representation becomes singular when the pitch angle reaches ±90º. Further investigation shows that quaternions avoid the singularity problem associated with Euler-angle representations. Therefore, they are widely used for spacecraft attitude representation and controller design [3-5]. The quaternion kinematic equation of the satellite is given in Eq (3).

$$\dot{Q}_h^b = \frac{1}{2} Q_h^b \otimes w_{hb}^b = \frac{1}{2} Q_h^b \otimes (w_{Ib}^b - C_h^b w_{Ih}^h) \tag{3}$$

where Q denotes the attitude quaternion of the spacecraft body-fixed frame (b) relative to the orbital frame h, expressed in the body-fixed frame b; where $\otimes$ denotes quaternion multiplication; where wb indicates the spacecraft's body-fixed frame b's angular velocity with respect to the orbital frame h; where w denotes the angular velocity of the spacecraft body-fixed frame b relative to the inertial frame I, expressed in the body-fixed frame b; where C denotes the coordinate transformation matrix from the orbital frame h to the body-fixed frame b, which is computed from the quaternion Q; where w denotes the orbital context h's angular speed with respect to the inertial frame I, represented in the orbital frame h.

2.4. Formulation of the control objective

In this study, an error quaternion is used to describe the deviation between the actual and desired attitudes. The desired attitude is represented using the conversion relationship between the direction cosine matrix and the quaternion [6-8]. Let QT denote the desired attitude quaternion, and Qe denote the attitude error quaternion. The error quaternion is calculated as follows:

$$QT\, Qe = Q \tag{4}$$

$$Q_e = Q_T^* Q \tag{5}$$

$$Q_T = \begin{pmatrix} q_{T0} \\ q_T \end{pmatrix}, Q_T^* = \begin{pmatrix} q_{T0} \\ -q_T \end{pmatrix} \tag{6}$$

DOI: 10.54254/2755-2721/2026.LD39410

Let the desired direction cosine matrix from the inertial frame to the spacecraft body-fixed frame be defined as:

$$C_l^b = \begin{bmatrix} C_{11} & C_{12} & C_{13} \\ C_{21} & C_{22} & C_{23} \\ C_{31} & C_{32} & C_{33} \end{bmatrix} \tag{7}$$

The desired direction cosine matrix is further converted into quaternion form. Let the desired attitude quaternion be denoted by

$$Q_T = [q_{1d} \quad q_{2d} \quad q_{3d} \quad q_{4d}]^T \tag{8}$$

$$S = 2\sqrt{1 + tr(C_I^b)} \tag{9}$$

$$q_{1d} = \frac{C_{23} - C_{32}}{S}, \quad q_{2d} = \frac{C_{31} - C_{13}}{S}, \quad q_{3d} = \frac{C_{12} - C_{21}}{S}, \quad q_{4d} = \frac{S}{4} \tag{10}$$

2.5. Control law design

After determining the desired attitude, it is necessary to further investigate how the actual spacecraft attitude tracks the desired attitude. The deviation between the actual and desired attitudes can be characterized by the attitude error. The objective of attitude control is to reduce this error under the applied control torque until it converges within an allowable range.

Therefore, the key issue in the subsequent controller design is to develop an appropriate attitude control law that enables the spacecraft to track the desired attitude rapidly and stably. A proportional-derivative (PD) controller is a widely used feedback controller in engineering control systems. Its basic principle is to construct the control input based on the error between the current and desired states and the rate of change of that error, thereby improving the dynamic response of the system.

The PD controller consists primarily of proportional and derivative terms. The proportional term generates a control action based on the current attitude error to accelerate error convergence. The derivative term provides damping based on the rate of change of the error, suppressing oscillations and improving system stability [9]. The control parameters are defined as follows:

$$T = u = I\dot{w} + w \times Iw = -K_p q_e - K_d w \tag{11}$$

The attitude control law of the spacecraft PD controller is then defined as: $T = -(Kpdq + Kdw)$.

3. Grey wolf optimization

Motivated by the communal structure and foraging habits of grey wolves, Mirjalili et al. [10] devised GWO, a swarm-intelligence optimisation algorithm. The hierarchical structure of a grey wolfpack is illustrated in Figure 5. The highest-ranking wolf is denoted by α , followed by β at the second level and δ at the third level, while the lowest-ranking wolves are denoted by ω . During the optimization process, higher-ranking wolves guide lower-ranking wolves toward promising regions of the search space where better solutions are more likely to be found.

DOI: 10.54254/2755-2721/2026.LD39410

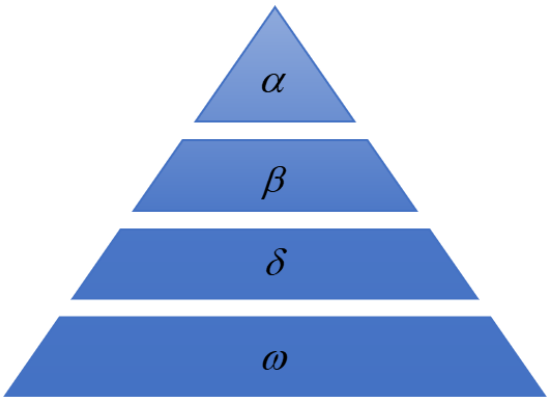


Figure 5. Hierarchical structure of the grey wolf social hierarchy

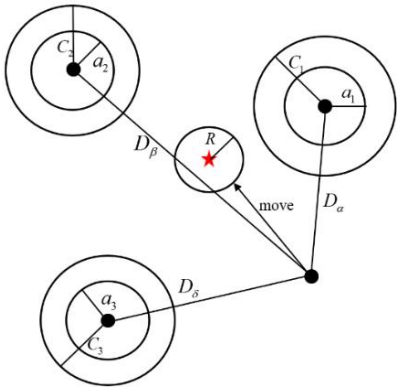


Figure 6. Individual tracking mechanism of the GWO algorithm

Let N denote the number of grey wolves and d denote the dimension of the search space. The i-th grey wolf's location in the d-dimensional search space can be written as xi = (xi1 , xi2 ,..., xid). The mathematical formulation of the GWO algorithm is described as follows:

$$D = \left| C \cdot X_p(t) - X(t) \right| \tag{12}$$

$$C = 2 \times r_1 \tag{13}$$

where t denotes the iteration index, Xp(t) is the prey's position vector at iteration t, X(t) is the grey wolf's location vector at iteration t, and D is the distance between a grey wolf and its prey. The coefficient C is an oscillation factor, and r_1 is a random number uniformly distributed over [0, 1]. The position of the grey wolf at iteration t+1 is updated according to Eq. (14):

$$X(t+1) = X_p(t) - A \bullet D \tag{14}$$

$$A = 2a \times r_2 - a \tag{15}$$

When the convergence factor, denoted by A, falls linearly from 2 to 0 as the number of iterations rises. The mechanism by which an individual wolf tracks the prey is illustrated in Figure 6.

The mathematical formulation of the prey-tracking mechanism is described as follows. The distances between an individual wolf and the α, β, and δ wolves are first calculated. Then, according to Eqs.(16)-(18), the movement direction of the individual wolf toward the prey is determined by combining the guidance information provided by the three leading wolves.

$$D_\alpha = \left| C_1 \cdot X_\alpha(t) - X(t) \right| \tag{16}$$

$$D_\beta = \left| C_2 \cdot X_\beta(t) - X(t) \right| \tag{17}$$

$$D_{\bar{\sigma}} = \left| C_3 \cdot X_{\bar{\sigma}}(t) - X(t) \right| \tag{18}$$

where D_α, D_β, and $D_{\bar{\sigma}}$ denote the distances between the remaining wolves in the pack and the three leading wolves, α, β, and δ, respectively. $X_\alpha(t)$, $X_\beta(t)$, and $X_{\bar{\sigma}}(t)$ represent the positions of

DOI: 10.54254/2755-2721/2026.LD39410

the three leading wolves, while C1, C2,and C3 are random vectors. X(t) denotes the current position of a grey wolf. The candidate position vectors X1, X2, and X3, which guide a ω wolf toward the α, β, and δ wolves, are calculated according to Eqs. (19)-(21):

$$X_1 = X_\alpha - A_1 \cdot D_\alpha \tag{19}$$

$$X_2 = X_\beta - A_2 \cdot D_\beta \tag{20}$$

$$X_3 = X_\delta - A_3 \cdot D_\delta \tag{21}$$

The final position of the ω wolf is given by:

$$X_p(t+1) = (X_1 + X_2 + X_3)/3 \tag{22}$$

Finally, when the prey can no longer escape, the wolves attack it and complete the hunting process, indicating that the global optimum has been found.

4. PD controller parameter optimization

PD controllers are widely used in spacecraft attitude control because of their simple structure and ease of implementation. However, their control performance is highly sensitive to the selection of controller parameters. Therefore, intelligent optimization algorithms can be employed for parameter tuning [11-13]. To improve both the automation of parameter tuning and the resulting control performance, a GWO- based PD controller parameter optimization method is developed in this study.

4.1. Initial parameter design

Because the HErO satellite is a small CubeSat with a relatively low mass, its inertia matrix is assumed to be:

$$I_B = \begin{bmatrix} 1.7 \times 10^{-3} & 0 & 0 \\ 0 & 1.7 \times 10^{-3} & 0 \\ 0 & 0 & 1.7 \times 10^{-3} \end{bmatrix} kg \cdot m^2 \tag{23}$$

The initial attitude quaternion is given by

$$Q_0 = [0.9893 \quad 0.0789 \quad 0.0941 \quad 0.0789] \tag{24}$$

The desired attitude quaternion is given by:

$$Q_T = [0.7641 \quad 0.1613 \quad 0.5597 \quad 0.2771] \tag{25}$$

The initial parameters of the PD controller are set as follows:

$$\begin{aligned} K_p &= [5 \quad 5 \quad 5] \\ K_d &= [5 \quad 5 \quad 5] \end{aligned} \tag{26}$$

The simulation time step is set to 0.01s, and the total simulation duration is 20 s.

DOI: 10.54254/2755-2721/2026.LD39410

4.2. Design of the optimization objective

The optimization variables are selected as the proportional and derivative gains along the three spacecraft body axes:

$$\mathbf{x} = [K_{p1}, K_{p2}, K_{p3}, K_{d1}, K_{d2}, K_{d3}]^T \tag{27}$$

Considering the attitude error, angular velocity error, and convergence speed, the following fitness function is constructed:

$$fitness = w_q J_q + w_\omega J_\omega + w_s t_s \tag{28}$$

where Jq denotes the integral term of the attitude error and is defined as:

$$J_q = \int_0^{t_f} \| \theta_e(t) \|_2 \mathrm{d}t \tag{29}$$

where tf denotes the final simulation time.

Because attitude control requires not only a reduction in attitude error but also the gradual decay and stabilization of the angular velocity, an integral term of the angular velocity error is introduced. Let

$$\boldsymbol{\omega}_{ob}^{b}(t) = [\omega_x(t) \quad \omega_y(t) \quad \omega_z(t)]^T \tag{30}$$

$$J_\omega = \int_0^{t_f} \| \omega_{ob}^{b}(t) \|_2 \mathrm{d}t \tag{31}$$

To evaluate the response speed of the system, the convergence time ts is further introduced. The system is considered to have converged when both the attitude error angle and the angular velocity norm enter their prescribed tolerance bands and remain within these bounds thereafter. The convergence time is defined as:

$$\mathrm{t_s} = \min\{\mathrm{t_k} \mid \theta_\mathrm{e}(\mathrm{t_j}) \le \varepsilon_\mathrm{q}, \omega_\mathrm{ob}^\mathrm{b}(\mathrm{t_j}) \le \varepsilon_\omega, \forall \mathrm{t_j} \ge \mathrm{t_k}\} \tag{32}$$

where εq denotes the threshold for the attitude error angle, and ε_ω denotes the threshold for the angular velocity error. In this study, these thresholds are set as follows:

$$\varepsilon_q = 0.5^\circ, \quad \varepsilon_\omega = 0.05^\circ/\mathrm{s}$$

The weighting coefficients of the individual terms in the fitness function are selected as follows:

$$w_q = 10, \quad w_\omega = 5, \quad w_s = 20$$

The configuration of the GWO parameters is as follows. The highest possible number of repetitions is set at fifty, while the population size is set at fifteen wolves. The optimization variables

DOI: 10.54254/2755-2721/2026.LD39410

are the six parameters of the PD controller. Their lower and upper bounds are specified as [0,0,0,0,0,0] and [50,50,50,50,50,50], respectively.

4.3. Optimization results

After 50 iterations, the convergence history of the fitness function is shown in Figure 7. During the optimization process, the fitness value decreases from 418.8833 to 100.12585.

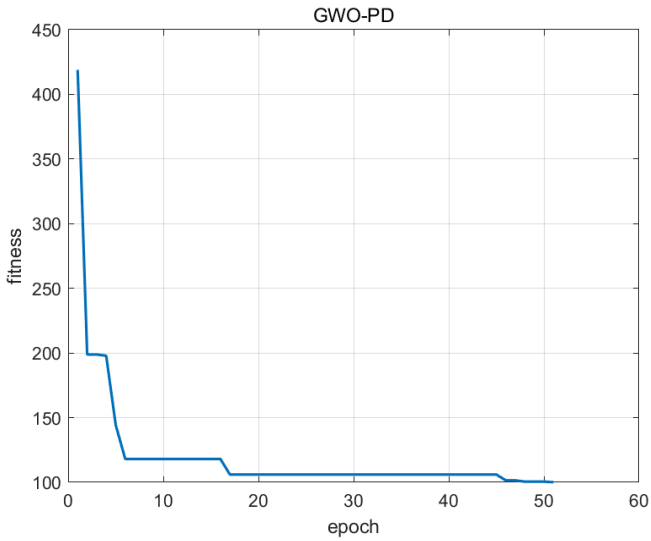


Figure 7. Iteration history of the GWO

The optimized parameters of the PD controller are:

$$\begin{aligned} K_p &= [25.37363 \quad 48.825349 \quad 46.905378] \\ K_d &= [6.4864 \quad 27.782771 \quad 26.510672] \end{aligned} \tag{33}$$

5. Scenario simulation

5.1. Observation window analysis

The HErO satellite was originally planned to be launched aboard the Kairos Rocket 3 on March 5, 2026, UTC, and inserted into a Sun-synchronous orbit (SSO). To estimate the initial time and approximate orbital position of HErO after orbital insertion and to provide a basis for subsequent simulation analysis, our research team communicated with SPACE ONE, the operator of Kairos Rocket 3. Based on the information obtained, an on-orbit operation and ground-observation simulation scenario for the HErO satellite was established using STK. The simulation starts at 00:00:00 UTC on March 6, 2026, and ends at 12:00:00 UTC on the same day, for a total simulation duration of 12 h.

DOI: 10.54254/2755-2721/2026.LD39410

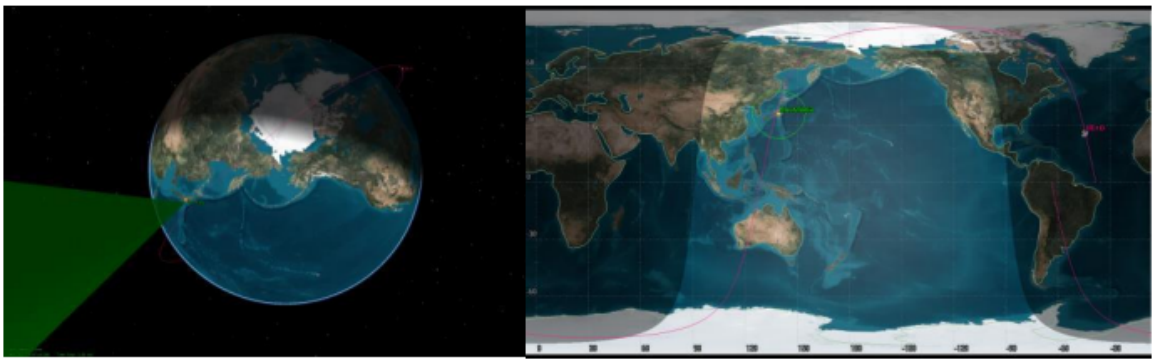


Figure 8. STK simulation scenario setup

The satellite's initial lunar characteristics are as follows: the semimajor axis is 7200 km, the eccentricity is 1e-6, the orbital inclination is 98.696 deg, the argument of perigee is 0 deg, the ascending the node's right elevation is 125 deg, and the true anomaly is 0 deg.

Our team selected Enoshima (35.29968ºN,139.480185ºE), Japan, as the ground observation site. To simulate the effective field of view of the ground-based observation equipment, a sensor is placed at the Enoshima observation site with a half-cone angle of 20 deg. The resulting STK simulation scenario is shown in Figure 8.

To ensure the validity of the subsequent attitude-pointing control simulation, the time window during which the HErO satellite passes through the observable region over Enoshima must first be determined. STK is used to analyze the visibility between the satellite and the ground-based observation sensor.

The results show that the HErO satellite enters the observable region at 00:40:06.484 UTC on March 6, 2026, and leaves the region at 00:41:06.235 UTC on the same day. The corresponding observation duration is approximately 59.75 s. Based on this observation window, the subsequent attitude-pointing control simulation is conducted over a 2h simulation period.

5.2. Desired attitude determination

To ensure that the LED-mounted surface of the HErO satellite remains stably pointed toward the ground observation station, the desired attitude is constructed based on the relative geometry between the satellite and the ground observation site. As illustrated in Fig. 4, let rp denote the position vector from the center of the Earth to the ground observation site. The unit line-of-sight vector from the satellite to the ground observation station is defined as:

$$\mathbf{e}_{\rho}^{I}=\frac{\mathbf{r}_{p}-\mathbf{r}_{b}}{\|\mathbf{r}_{p}-\mathbf{r}_{b}\|} \tag{34}$$

Because the mission requires the +Zb-axis of the spacecraft body-fixed frame to point toward the ground observation station, the third axis of the desired attitude frame is defined as:

$$\mathbf{b}_{3d}^{I}=\mathbf{e}_{\rho}^{I} \tag{35}$$

The pointing constraint on the +zb -axis alone cannot uniquely determine the spacecraft rotation about the line-of-sight direction. Therefore, the spacecraft velocity direction is selected as an auxiliary reference direction and projected onto the plane

perpendicular to bd. The desired +Xb-axis direction is then obtained as:

DOI: 10.54254/2755-2721/2026.LD39410

$$b_{1d}^{I} = \frac{v_b^I - (v_b^I \cdot b_{3dI}^I) b_{3d}^I}{v_b^I - (v_b^I \cdot b_{3dI}^I) b_{3d}^I} \tag{36}$$

The desired +Yb-axis direction is then determined according to the right-hand rule:

$$\mathbf{b}_{2d}^{I} = \mathbf{b}_{3d}^{I} \times \mathbf{b}_{1d}^{I} \tag{37}$$

The desired direction cosine matrix from the inertial frame to the spacecraft body- fixed frame is then obtained as:

$$\mathbf{C}_I^b = \begin{bmatrix} \left(\mathbf{b}_{1d}^{I}\right)^T \\ \left(\mathbf{b}_{2d}^{I}\right)^T \\ \left(\mathbf{b}_{3d}^{I}\right)^T \end{bmatrix} \tag{38}$$

The desired attitude obtained from the above calculation is shown in Figure 9.

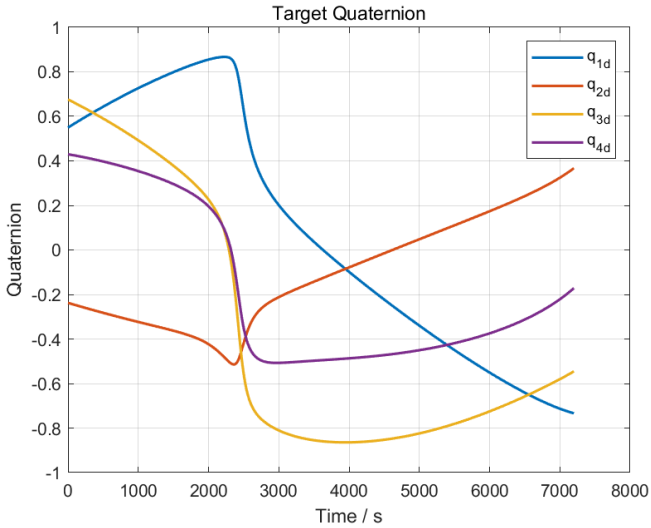


Figure 9. Desired on-orbit attitude of the HErO satellite

5.3. Results and analysis

Using the PD attitude controller designed in Section 4, the desired-attitude tracking performance of the HErO satellite is evaluated over a 2 h simulation period. During the simulation, the desired attitude is determined from the satellite position, the ground observation site, and the spacecraft velocity direction. The primary control objective is to keep the +Zb-axis of the spacecraft body-fixed frame stably pointed toward the ground observation site. This ensures that the satellite surface carrying the LED remains oriented toward the region where the ground experiment team is located.

As shown by the attitude-tracking results in Figure 10, the actual spacecraft attitude follows the desired attitude well. At the beginning of the simulation, a brief transient response occurs because of the initial deviation between the actual and desired attitudes. Under the action of the controller, the actual attitude gradually converges toward the desired attitude and maintains good tracking

DOI: 10.54254/2755-2721/2026.LD39410

performance during the subsequent flight. These results indicate that the designed PD controller effectively suppresses the influence of the initial attitude deviation and enables the spacecraft to satisfy the mission pointing requirements.

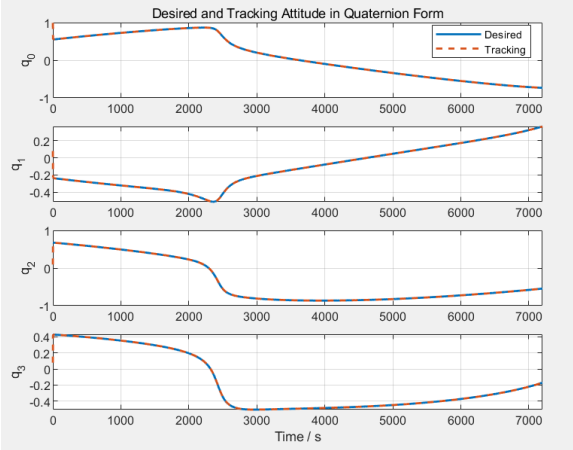


Figure 10. Attitude-tracking results

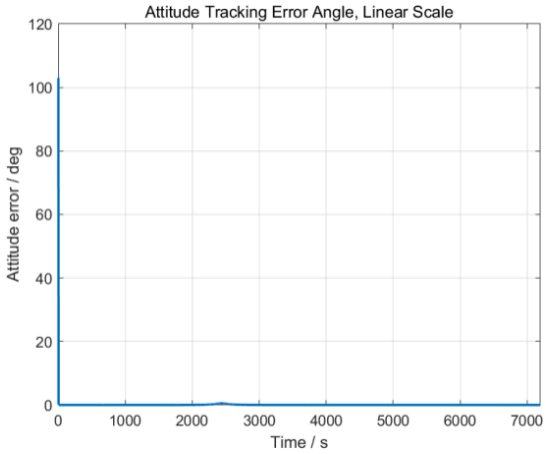


Figure 11. Pointing deviation of the spacecraft +Zb-axis

To further evaluate the Earth-pointing performance of the LED-mounted surface, the angle between the spacecraft +Zb-axis and the line-of-sight direction from the satellite to the ground observation site is calculated and used as the pointing-deviation metric. A smaller angle indicates that the +Zb-axis is more closely aligned with the ground observation site, corresponding to higher pointing accuracy of the LED-mounted surface. As shown in Figure 11, the angle between the spacecraft +Zb-axis and the line of sight to the ground observation site remains within a small range throughout the 2h simulation period. This indicates that the satellite can continuously maintain the LED-mounted surface oriented toward the ground observation site.

In particular, as the satellite approaches and enters the observation window over Enoshima, no significant increase in pointing deviation is observed. This result demonstrates that the controller satisfies the attitude-stability requirements of the observation mission.

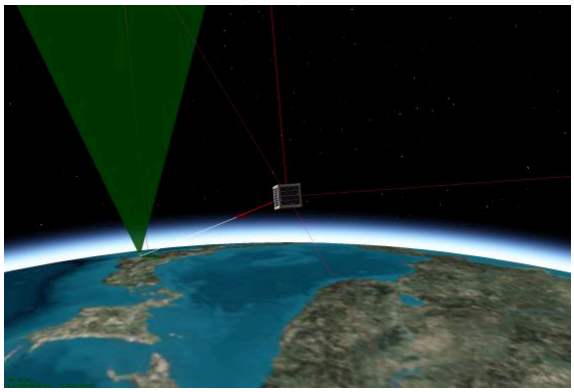


Figure 12. HErO satellite approaching the observation site



Figure 13. HErO satellite entering the observation region

DOI: 10.54254/2755-2721/2026.LD39410

For a more intuitive verification of the attitude-control results, the attitude data obtained from the MATLAB simulation are further imported into STK. The spacecraft body axes, ground observation site, and field of view of the observation sensor are then displayed in the STK three-dimensional scenario.

As shown in Figures 12&13, as the satellite approaches the observation region and enters the coverage area of the ground observation sensor, the spacecraft +Zb-axis remains pointed toward the Enoshima ground observation site. The pointing relationship observed in STK is consistent with the desired-attitude determination and attitude-control simulation results obtained in MATLAB.

6. Conclusions and future work

This study addresses the requirements of the LED-based optical communication mission of the HErO satellite developed at Hiroo Gakuen. The optimization and simulation-based validation of an attitude controller for a small satellite are investigated. The mission requires the LED-mounted surface of HErO to remain stably pointed toward the ground observation site while the satellite passes through the observable region.

First, the models of spacecraft attitude dynamics and quaternion kinematics are established. Then the target orientation is formed from the satellite position, velocity and ground observation point. A proportional-derivative (PD) controller is the fundamental component of the attitude control system. Then the GWO is used to tune the proportional and derivative gains along the three body axes, so as to improve the attitude response speed and tracking stability.

The simulation results show that the GWO-tuned PD controller effectively improves the attitude response performance and enables the actual spacecraft attitude to track the desired attitude accurately. In the MATLAB simulation, the angle between the spacecraft +Zb-axis and the line of sight from the satellite to the ground observation site remains within a small range. This indicates that the LED-mounted surface can continuously point toward the ground observation site.

The attitude data are further imported into STK for three-dimensional visualization. The results show that the spacecraft +Zb-axis remains stably pointed toward the ground observation region as the satellite approaches and enters the observation region over Enoshima. These results verify the feasibility of the proposed attitude control method for the HErO satellite mission scenario.

Several aspects of this study can be further improved. Firstly, the current fitness function mainly takes attitude error, angular velocity error and convergence time into account. Future work could include mission related metrics like control-torque consumption, actuator capability constraints, and pointing accuracy during the observation window. This would give the controller parameters more consistent with the practical engineering requirements.

In addition, only the GWO is employed in this study to optimize the PD controller parameters. The proposed approach can be compared with particle swarm optimization, genetic algorithms, differential evolution and multiobjective optimization methods [14, 15] in the future work. Then the convergence speed, global optimization ability and parameter robustness for HErO satellite attitude control could be have been evaluated systematically [16] and provide a more complete reference for future design of small-satellite attitude controllers.

References

[1] Rajamani, R. (2012). *Vehicle dynamics and control* (2nd ed.). New York: Springer. DOI: 10.1007/978-1-4614-1433-9.

[2] Markley, F. L., & Crassidis, J. L. (2014). *Fundamentals of spacecraft attitude determination and control*. New York: Springer.

DOI: 10.54254/2755-2721/2026.LD39410

[3] Wertz, J. R. (1978). *Spacecraft attitude determination and control*. Dordrecht: D. Reidel Publishing Company.
[4] Schaub, H., & Junkins, J. L. (2003). *Analytical mechanics of space systems*. Reston: American Institute of Aeronautics and Astronautics.
[5] Chaturvedi, N. A., Sanyal, A. K., & McClamroch, N. H. (2011). Rigid-body attitude control. *IEEE Control Systems Magazine, 31*(3), 30–51. DOI: 10.1109/MCS.2011.940459.
[6] Wie, B., & Barba, P. M. (1985). Quaternion feedback for spacecraft large angle maneuvers. *Journal of Guidance, Control, and Dynamics, 8*(3), 360–365. DOI: 10.2514/3.19988.
[7] Klumpp, A. R. (1976). Singularity-free extraction of a quaternion from a direction cosine matrix. *Journal of Spacecraft and Rockets, 13*(12), 754-755. DOI: 10.2514/3.27947.
[8] Younes, A. B. (2019). Derivation of all attitude error governing equations for attitude error representations. *Sensors, 19*(21), 4682. DOI: 10.3390/s19214682.
[9] Su, Y., & Zheng, C. (2021). Single saturated PD control for asymptotic attitude stabilisation of rigid bodies. *IET Control Theory & Applications*. DOI: 10.1049/iet-cta.2020.0598.
[10] Mirjalili, S., Mirjalili, S. M., & Lewis, A. (2014). Grey wolf optimization. *Advances in Engineering Software, 69*, 46-61. DOI: 10.1016/j.advengsoft.2013.12.007.
[11] Zhang, Z. B., Li, X. H., An, J. P., Man, W. X., & Zhang, G. H. (2020). Model-free attitude control of spacecraft based on PID-guide TD3 algorithm. *International Journal of Aerospace Engineering, 2020*, 8874619. DOI: 10.1155/2020/8874619.
[12] Qi, Y., Jing, H., & Wu, X. (2022). Variable structure PID controller for satellite attitude control considering actuator failure. *Applied Sciences, 12*(10), 5273. DOI: 10.3390/app12105273.
[13] Sayin, E., Bitirgen, R., & Bayezit, I. (2023). Attitude control and parameter optimization: A study on Hubble Space Telescope. *Measurement Science Review, 23*(4), 146-153. DOI: 10.2478/msr-2023-0019.
[14] Kennedy, J., & Eberhart, R. (1995). Particle swarm optimization. *Proceedings of ICNN'95 - International Conference on Neural Networks*, 1942-1948. DOI: 10.1109/ICNN.1995.488968.
[15] Storn, R., & Price, K. (1997). Differential evolution – A simple and efficient heuristic for global optimization over continuous spaces. *Journal of Global Optimization, 11*, 341-359. DOI: 10.1023/A:1008202821328.
[16] Adnane, A., Boukallel, M., & Bourahla, M. (2024). CubeSat attitude stabilization via dual-loop control. *Proceedings of the 2024 International Conference on Artificial Intelligence, Computer, Data Sciences and Applications*. DOI: 10.1145/3651781.3651835.